European Journal of Mechanics / A Solids 117 (2026) 106021

Contents lists available at ScienceDirect

European Journal of Mechanics / A Solids

journal homepage: www.elsevier.com/locate/ejmsol

Full Length Article

A deep learning approach to predict cyclic softening behaviour of irradiated and non-irradiated RAFM steels under low cycle fatigue

Hussein Zahran [a,b,c], Aleksandr Zinovev [a], Dmitry Terentyev [a], Ali Aouf [d,e], Magd Abdel Wahab [b,f,g,*]

[a] Structural Materials Group, Institute for Nuclear Energy Technology, Belgian Nuclear Research Centre SCK CEN, Mol, 2400, Belgium
[b] Soete Laboratory, Department of Electrical Energy, Metals, Mechanical Constructions and Systems, Faculty of Engineering and Architecture, Ghent University, 9000, Ghent, Belgium
[c] Department of Design and Production Engineering, Faculty of Engineering, Ain Shams University, Cairo, Egypt
[d] Engineered and Geosystems Analysis Group, Institute of Sustainable Waste and Decommissioning, Belgian Nuclear Research Centre SCK CEN, Mol, 2400, Belgium
[e] Université Catholique de Louvain, 1348, Louvain-la-Neuve, Belgium
[f] College of Engineering, Yuan Ze University, Taiwan
[g] Parallel and Distributed Systems Laboratory, Jožef Stefan Institute, Jamova Cesta 39, SI-1000, Ljubljana, Slovenia

ARTICLE INFO

Keywords:
EUROFER97
Machine learning
SHAP analysis
Deep neural network
Fusion materials

ABSTRACT

Qualification of Reduced Activation Ferritic-Martensitic (RAFM) steels for fusion reactors require Low Cycle Fatigue (LCF) testing including experiments after irradiation. Cyclic softening curves from these tests help reduce the conservatism of RCC-MRx. In this work, Deep Neural Network (DNN) is used to predict the cyclic softening curves for irradiated and non-irradiated RAFM steels. Cyclic softening for specimens tested under different conditions are gathered from literature. Three samples are used in this study with increased number of points obtained per curve. The results showed that increasing the number of points per curve reduced the overfitting of the training set. This is shown through the increase of the accuracy scores for both the validation and prediction sets. SHapley Additive exPlanation (SHAP) analysis is performed to understand how the DNN model interprets the effect of the input features on the output. The DNN model with the tuned hyperparameters is used to predict the cyclic softening curves of the prediction sets. The curves show very good agreement between the experimental and predicted curves for both irradiated and non-irradiated material.

1. Introduction

Knowledge of the cyclic softening behaviour of a structural material is of high importance to the safe and efficient design of components subject to cyclic loading. During cyclic loading, many alloys exhibit a gradual reduction in stress which can significantly influence fatigue life, structural stability, and failure modes. Accurate prediction of cyclic softening enables engineers to anticipate material degradation, optimize design margins, and schedule planned maintenances preventing premature failures. Therefore, this knowledge enhances both safety and cost-effectiveness of engineering systems (Zhang et al., 2009; Lopez and Fatemi, 2012; Zhou et al., 2018).

Structural materials in In-Vessel Components (IVCs) of fusion reactors such as ITER and DEMO are expected to face thermomechanical fatigue. The cyclic nature of the tokamak operation in these reactors with frequent startups and shutdowns in addition to the plasma instabilities (Spolladore et al., 2023; Lehnen et al., 2015) leads to Low Cycle Fatigue (LCF) with varying strain amplitudes (Marmy and Kruml, 2008). The qualification of candidate materials for these structural components requires an understanding of their performance under LCF especially under relevant neutron irradiation doses.

Reduced Activation Ferritic Martensitic (RAFM) steels are the main candidate steels for the structural components in IVCs due to their reduced neutron activation during operation aiming at high tensile, and creep strengths (Lindau et al., 2005; van der Schaaf et al., 2003; Chernov et al., 2007; Huang and Team, 2014; Mergia and Boukos, 2008). EUROFER97 is the main European candidate for the test blanket module (TBM) in ITER, and for the breeding blanket in DEMO. These RAFM

* Corresponding author. Soete Laboratory, Department of Electrical Energy, Metals, Mechanical Constructions and Systems, Faculty of Engineering and Architecture, Ghent University, 9000, Ghent, Belgium.
E-mail address: magd.abdelwahab@UGent.be (M. Abdel Wahab).

https://doi.org/10.1016/j.euromechsol.2026.106021
Received 15 March 2025; Received in revised form 24 May 2025; Accepted 7 January 2026
Available online 8 January 2026

Table 1
Materials and LCF test conditions included in the gathered database with their sources.

Material	Specimen diameter (mm)	Test medium	Irradiation/test temperature (° C)	Irradiation dose (dpa)	Strain ranges (%)	Source
E97-1	2	Air	300	2.5	1.40	Luzginova et al. (2011)
			330	30.2	0.81, 0.91, 1.01	Petersen (2010)
				71	0.80, 0.90, 1.0, 1.10	Gaganidze and Petersen (2011)
		Vacuum	250	–	0.40, 0.50, 0.55, 0.60, 0.70, 0.90, 1.0	Materna-Morris et al. (2013)
				16.3	0.50, 0.60, 0.70, 0.80, 0.90, 1.0	
			350	–	0.45, 0.50, 0.60, 0.70, 0.80, 0.90	
				16.3	0.60, 0.70, 0.80	
			450	–	0.35, 0.40, 0.50, 0.60, 0.70, 0.90	
				16.3	0.35, 0.40, 0.50, 0.60, 0.70, 0.80	
	2.7	Air	20	–	0.80	Marmy and Kruml (2008)
		Vacuum	150		0.50, 0.80	
			300			
			550			
	8.8	Air	500	–	0.40, 0.70, 1.0, 1.50	Fernández (2004)
E97-2	2	Air	330	30.2	0.81, 0.92, 1.01, 1.21	Petersen (2010)
				71	0.80, 0.90, 1.0, 1.10	Gaganidze and Petersen (2011)
			550	–	0.60, 1.0, 1.60	(Aktaa et al., 2020; Roldán et al., 2019)
	8.8	Air	20	–	0.60, 0.80, 1.0, 1.40, 1.80	Roldán et al. (2019)
			550		0.40, 0.50, 0.60, 0.80, 1.0, 1.40, 1.80	(Roldán et al., 2019; Zhang et al., 2020)
E97-3	5	Air	20	–	0.60, 0.80, 1.0, 1.20, 1.50	(Zahran et al., 2024; Zinovev et al., 2024)
			350		0.60, 0.74, 1.0, 1.20, 1.50	
	8.8	Air	550	–	0.40, 0.60, 0.80, 1.0, 1.50	Zinovev et al. (2024)
F82H	2	Air	330	30.2	0.80, 0.90, 1.0	Petersen (2010)
	8	Air	400	–	0.50, 0.75, 1.0	Nozawa et al. (2021)
			550			
		Vacuum	550	–	0.60, 1.0, 1.5	Hirose et al. (2018)
CLAM	6	Air	450	–	0.80, 1.0, 1.60	Zhao et al. (2016)
			550			
	8	Air	20	–	0.50, 1.0, 1.60, 2.60, 4.0	Hu et al. (2013)
			550		0.35, 0.50, 0.60, 0.90, 1.20, 2.40, 3.60	Hu et al. (2014)
In-RAFM	10	Air	20	–	1.20	Mariappan et al. (2016)
			400			
			450			
			550		0.50, 0.80, 1.20, 2.0	
			600		1.20	

steels experience softening during cyclic operation. Continuous cyclic loading leads to significant microstructural changes and pronounced cyclic softening, which can adversely affect creep resistance, swelling, and segregation phenomena during irradiation (Giordana et al., 2011a; Oh et al., 2021a; Aktaa and Schmitt, 2006; Kim et al., 2009). Therefore, several LCF experiments need to be performed on RAFM steels on non-irradiated and irradiated (up to relevant doses) specimens. This could be challenging due to the technical difficulties and the high cost of performing LCF under neutron irradiation.

EUROFER97 experiences non-negligible creep at temperatures exceeding 375 °C regardless the holding time (Garcia et al., 2020; Muscat et al., 2023). This temperature is expected to be within the operation range of the structural components in the breeding blankets (Mahler and Aktaa, 2018). For these reasons, the knowledge of the cyclic softening curves of RAFM steels is beneficial for the design team. For instance, a creep-fatigue assessment tool was developed by KIT (Aktaa et al., 2019) considering the effect of cyclic softening on the creep rupture time. This is done by calculating the cyclic softening (ψ) as a ratio between peak stress at a given cycle and the peak stress in the first cycle, from which the cyclic softening factor $K\psi$ (ratio of the creep strength of as-received material to that of the cyclic softened material) can be calculated to determine the allowable creep time from design creep curves.

The availability of cyclic softening curves under different loading conditions is important for the application of these design rules. With the previously mentioned difficulties, an alternative way to predict the cyclic softening behaviour of RAFM steels under conditions that have not yet been tested would be an important asset (Tanigawa, 2018).

Several studies were performed modelling the cyclic softening behaviour of RAFM steels using numerical simulations either using micromechanical or macroscopic viscoplasticity models (Aktaa and Schmitt, 2006; Führer and Aktaa, 2018; Aktaa and Petersen, 2009a, 2009b, 2011; Msolli, 2014; Giordana et al., 2011b; Zahran et al., 2024). The challenge with these models is the computational time required to parametrize them. In addition to this, these models require the availability of several LCF experiments under each test condition to accurately model the cyclic softening behaviour under different strain ranges. This becomes difficult when it comes to the availability of the LCF experiments for irradiated specimens as mentioned before.

Machine Learning (ML) models have widely been used for regression and function approximation. One of these models is Artificial Neural Network (ANN), which is capable to fit non-linear relations with multiple variables (Mortazavi and Ince, 2020). ANN has been used in several areas including microstructural analysis (de Albuquerque et al., 2008, 2009), and fatigue failure (Barbosa et al., 2020a; He et al., 2021; Dong et al., 2025; Wang et al., 2023). The prediction of fatigue failure was done either on the fatigue life of metallic alloys as individual points or in the form of predicting the S–N curves for specific alloys. For instance,

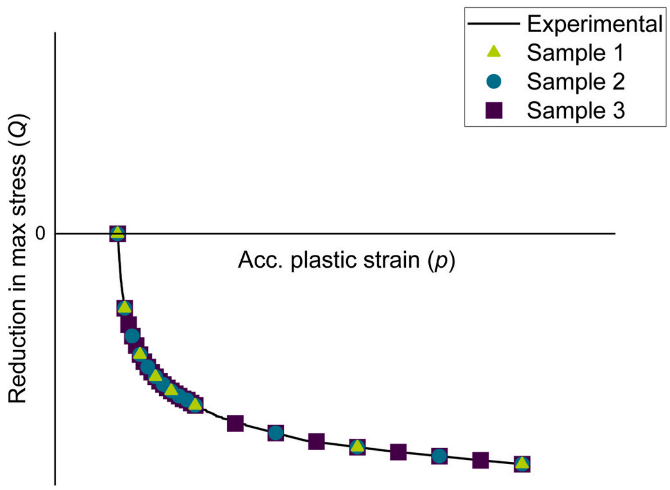

Fig. 1. Typical cyclic softening curve with the distribution of points extracted per curve for samples 1, 2, and 3.

the study by Lian et al. (2022) predicted the S–N curves of aluminium alloys by using knowledge based ML. With this technique, the knowledge from empirical formulas was transferred to the ML model in order to enhance the accuracy of prediction. Another study by Zhou et al. (2023) predicted the S–N curves of various metallic alloys using a probabilistic physics informed neural network. This technique helped avoid the overfitting of the training data. In another study, Zhang et al. (2021) employed conventional ML models, including RF, artificial neural networks (ANN), and SVM, alongside deep learning to predict the fatigue, creep, and creep-fatigue life of 316 austenitic stainless steel at high temperatures, showing deep learning's superior performance in prediction accuracy and generalization ability.

The use of ML in the prediction of the fatigue behaviour of metallic alloys was restricted to the prediction of fatigue life, endurance limit, and fatigue crack propagation. There was no study in literature predicting the cyclic softening of metallic alloys despite its importance in reducing the conservatism in design as discussed earlier.

Several studies were performed predicting the irradiation-induced change in the mechanical properties of RAFM steels, including the changes in tensile and impact properties after irradiation to doses relevant to fusion reactors (Long and Zhao, 2020; Wang et al., 2020a, 2020b; Sai et al., 2023; Li et al., 2022; Liu et al., 2022). A previous study by the authors predicted the fatigue life of irradiated and non-irradiated RAFM steels using ML (Zahran et al.). No other studies were found on the prediction of fatigue behaviour of metallic alloys after irradiation.

The aim of this study is to predict the cyclic softening curves of irradiated and non-irradiated RAFM steels under different test conditions using Deep Neural Network (DNN). This should help reduce the conservatism of RCC-MRx and aid the design team during their choice of the candidate steels for structural materials in the IVCs. In this study, the gathered fatigue dataset is introduced in section 2. This is followed by section 3 with a description of the used DNN model, and the framework for its hyperparameter tuning and training. Finally, the results of the training and validation, and the prediction for unseen test conditions are shown in section 4.

2. Dataset establishment

Cyclic softening curves were gathered from literature for different RAFM steels tested under various LCF test conditions. The RAFM steels included in this study were EUROFER97 (Gaganidze et al., 2018), F82H (Jitsukawa et al., 2002), CLAM (Huang and Team, 2014), and In-RAFM (Albert et al., 2016). The three produced batches of EUROFER97, for which LCF data was found in literature are denoted as “E97-1”, “E97-2”, and “E97-3” in the present manuscript. The data obtained on 160 LCF specimens of irradiated and non-irradiated material were selected for this study based on the availability of the cyclic softening curves.

The inputs to the DNN model predicting the cyclic softening curves were chosen based on the previous work dedicated to the prediction of the fatigue life of RAFM steels using ML (Zahran et al.), where the consideration of yield strength was shown not to have significant impact on the accuracy of prediction of fatigue life. For this reason, the tensile properties were not chosen as an input feature. The inputs were the specimen diameter, the test medium, the irradiation/test temperature, the irradiation dose, and the strain range. The strain ratio of all the LCF tests included in this database was −1 (symmetric LCF tests). The materials and test conditions included in the database are shown in Table 1. It is important to mention that for irradiated specimens, the test temperature was always the same as the irradiation temperature. Therefore, they were merged in one column of the table.

The modelling of cyclic softening in finite element analysis (viscoplasticity modelling) is usually done through the isotropic hardening variable as a function of the accumulated plastic strain. This variable represents the change in the yield function radius. Hence, the gathered cyclic softening curves were rebuilt in the form of Q as a function of p, as shown in Fig. 1, where Q is the change in maximum stress per cycle compared to the first cycle and p is the accumulated plastic strain Q represents the cyclic softening of the material, its value starts at 0 in the first cycle. Q attains a slight positive value in the first few cycles in the tests in which the specimen experienced slight cyclic hardening, and afterwards steadily decreases below zero in the following cycles. In other words, the lower the value of Q, the more cyclic softening the material has exhibited.

In order to fit this definition, the gathered cyclic softening curves listed in Table 1 in the form of maximum stress vs cycle were transformed into Q-p by the calculation of the Q as the maximum stress at a given cycle minus the maximum stress in the first cycle. The Q-p curves were built up to half-life only where cyclic softening effect rather than damage mechanics is dominant. The plastic strain per cycle (Δp) was estimated from the maximum stress (σ_{max}) in this cycle using the following equation (Narendra et al., 2019):

$$\Delta p = \Delta \varepsilon - \frac{2\sigma_{max}}{E} \tag{1}$$

where $\Delta\varepsilon$ is the test strain range, and E is the Young's modulus of the material.

Three samples were used in this study in terms of the number of points per curve. 8 points per curve, 15 points per curve, and 26 points per curve represent samples 1, 2, and 3 respectively which is demonstrated in Fig. 1. It is important to mention that for each of the samples, the points are more densely placed in the first part of the cyclic softening curve compared to the rest. This helps better describe the curvature with the significant increase in cyclic softening in the first cycles compared to the less significant linear cyclic softening for the rest of the cycles. Having data from 160 LCF specimens, sample 1 included 1280 datapoints, sample 2 included 2400 datapoints, and sample 3 included 4160 datapoints in total.

3. Machine learning framework

3.1. Deep neural network approach

An Artificial Neural Network (ANN) is a machine learning technique inspired neurons communicate in the human brain. It is particularly effective for solving non-linear and complex problems by learning patterns from data (Zhao et al., 2023). The DNN extracts the relationship between the different input features to predict targets in a generalized manner which helps predict unknown targets (Barbosa et al., 2020b).

A typical ANN is model consists of several layers, with each layer

Table 2
Range of values used for tuning the DNN hyperparameters and their best values.

Hyperparameter	Range for tuning	Best value
Number of hidden layers	1–4	3
Number of neurons in each hidden layer	8–256	64

consisting of operational neurons. These layers are interconnected with weight coefficients. The input layer and the output layer contain number of neurons equal to the number of input features and output targets, respectively. In between, there are one or more hidden layers with number of neurons exceeding the ones in the input and output layers. The number of hidden layers and the number of neurons in each hidden layer were selected based on systematic hyperparameter tuning using grid search and cross-validation. A large number of hidden layers or neurons is capable of solving complex problems, however, may lead to overfitting of the training set with an insufficient number or size of training samples, while too few may underfit the training set. (Bejani and Ghatee, 2021).

A Deep Neural Network (DNN) refers to an ANN architecture with more than two hidden layers, allowing for greater model depth and the ability to capture more complex feature interactions. The optimum number of hidden layers was found to be three (Table 2), as this configuration consistently yielded the lowest validation loss across multiple runs using K-fold cross-validation and GridSearchCV tuning.

The DNN model used in this study is a feed forward model with the signal feeding from the input layer to the output layer. Each neuron has its weight coefficients and is activated with an activation function. Rectified Linear Unit (RELU) activation function was used due to its fast computation and it avoids the vanishing gradient problem (Halamka et al., 2023). This is coupled with back propagation optimization which feeds the error between the output of the model, and the experimental values backwards to update the weight coefficients during the training process. In this study, Adam optimizer which combines first and second-order gradient descent is used for faster convergence (Gao et al., 2024). The choice of the learning rate should be done with care as a small learning rate might slow down the training process while a large value might lower the probability of convergence (Wong and Kim, 2018). Here, a learning rate of 0.001 was selected after comparative testing across standard values (e.g., 0.1, 0.01, 0.001, 0.0001). This value provided the best trade-off between convergence speed and model stability, as reflected by minimized validation loss.

The architecture of the implemented DNN model is shown in Fig. 2. The input layer consists of six neurons for the input features: specimen diameter, irradiation/test temperature, test medium, irradiation dose, strain range, and the accumulated plastic strain (p). The output layer consists of one neuron for one target variable: maximum stress reduction (Q). The number of hidden layers and the number of neurons were tuned as discussed in the following section.

3.2. Hyperparameter tuning

The DNN model was implemented using 'pytorch' python package (Paszke et al., 2019). The first step was to preprocess the input data, which involved cleaning the dataset, encoding categorical variables, and scaling all numerical inputs to a standard normal distribution. To

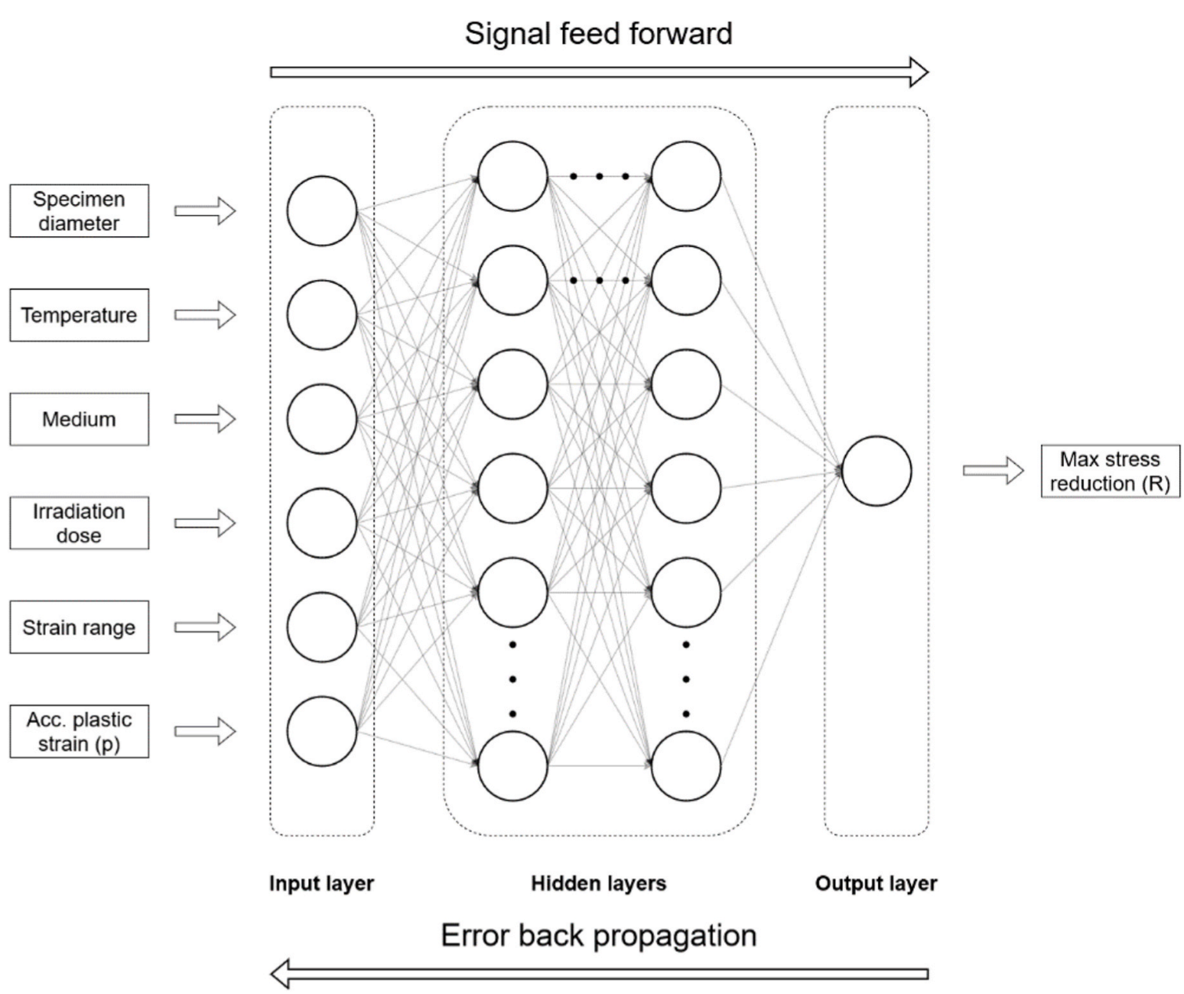

Fig. 2. Architecture of the DNN model.

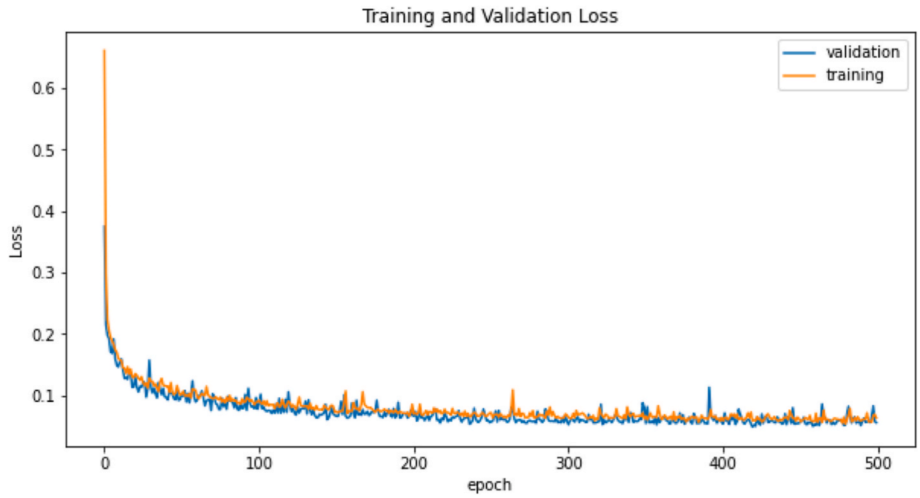

Fig. 3. MSE loss with epochs for training and validation sets (sample 1).

overcome any skewness in the distribution of the input features or target, their values were standardized using the StandardScaler function from the scikit-learn library, which transforms data to have a mean of 0 and a standard deviation of 1. This ensures that all features contribute equally during training, preventing bias due to differing scales. (Pedregosa et al., 2011). The idea was to scale all the features to look like standard normal distribution with zero mean and unit variance. This helps prevent any feature from dominating the objective function and hence from influencing the training results.

The cyclic softening curves in the gathered dataset were initially divided into training, validation, and prediction sets with percentages of 70 %, 15 %, and 15 % respectively. The training set was used for training the model, and the validation set was used to ensure that the training was done properly with no overfitting of the training set. Overfitting means that the model only learns the training data and has limited generalization capabilities. Thus, the accuracy scores were compared between the training and the validation sets and the best-tuned model was selected as the one with the lowest difference in performance between training and validation sets, evaluated using Mean Squared Error (MSE) as the primary metric. Finaly, the prediction set was not included in the training process and used only in the end to check the ability of the trained model to predict the cyclic softening curves of unseen test conditions.

The prediction capability of a ML model depends on the choice of its hyperparameters. As mentioned in section 3.1, the hyperparameters of the DNN models to be tuned are the number of hidden layers and the number of neurons in each hidden layer. The initial range of these hyperparameters were defined based on the number of input features, and the number of datapoints. GridSearchCV from the scikit-learn library (Pirjatullah et al., 2021) was then used for fine-tuning. GridSearchCV tests all different combinations of hyperparameters evaluating the model performance using each combination. The result would be the hyperparameters giving the best accuracy scores on the training set.

Hyperparameter tuning with GridSearchCV utilizes the K-fold Cross-Validation method (Jung, 2017). The training set is divided into k parts: k-1 parts are used for sub-training, and the last part is used for validation. This process is repeated k-times with each time changing the part used for validation every time adjusting the hyperparameters until the final choice is reached. The Mean Squared Error (MSE) score presented in section 3.3 was used as an evaluation for the model performance during tuning.

Table 2 shows the range of hyperparameters used and the best combination reached for this study. The best combination was found to be in the middle of the provided range. The same combination was found to be best for all three samples.

3.3. DNN model training

After the hyperparameter optimization, the final DNN model with the tuned hyperparameters was trained separately using the training set in the three samples. In each epoch, model weights were updated using the Adam optimizer and the training loss was computed using the MSE function. The batch size used was 32 and 500 epochs were used to reach the best performance of the model. In each epoch, the model was trained using the training set, then validation set was predicted using the trained model. Again, MSE loss was used as an accuracy score. Fig. 3 shows the decrease in MSE loss with epochs for both the training and validation sets for sample 1. A similar curve was obtained for the other two samples. This figure shows that the minimum loss was already reached, and beyond this point, continued training caused the validation loss to stagnate or increase while training loss continued to decrease, an indication of overfitting. This behavior was used as a practical stopping criterion. The small fluctuations observed in the loss curves reflect the inherent variability (stochasticity) in the dataset and are consistent with the known scatter in fatigue behaviour. This further supports the relevance of using probabilistic modelling approaches like machine learning. (Farid, 2022).

As the model performance might differ from one run to another, the training was done 10 times for every sample, the training and validation accuracy scores were computed for every run. The scatter of the accuracy scores was also used to assess the performance of the model.

The accuracy of the model was assessed using R^2 and MSE scores. These scores were calculated as follows:

$$R^2 = 1 - \frac{\sum_{i=1}^{N}\left(Q_i - Q_i^{pred}\right)^2}{\sum_{i=1}^{N}\left(Q_i - \overline{Q}\right)^2} \tag{2}$$

$$MSE = \frac{1}{N}\sum_{i=1}^{N}\left(Q_i - Q_i^{pred}\right)^2 \tag{3}$$

where Q_i is the experimental value of the maximum stress reduction, Q_i^{pred} is the predicted value by DNN, and $\overline{Q}$ is the average of the experimental values in the set. N represents the number of datapoints in the set.

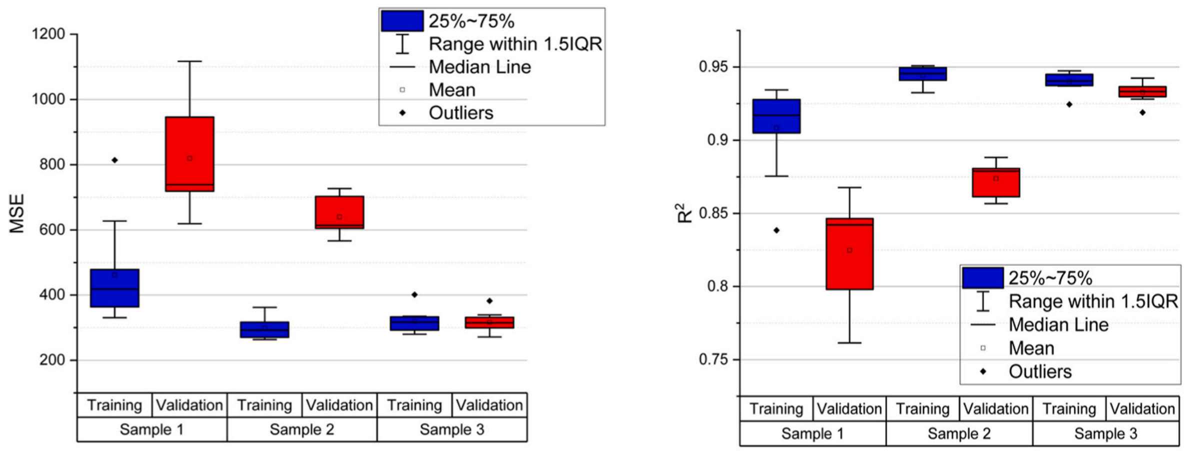

(a) (b)

Fig. 4. Accuracy scores for the prediction of the DNN on the training and validation sets: (a) MSE, and (b) R^2.

Table 3
Computational time and accuracy scores of the three samples.

Sample	Running time (s)		MSE (MPa^2)		R^2	
			Training	Validation	Training	Validation
1	36	Mean	462	820	0.9084	0.8249
		SD	150	164	0.0298	0.0350
2	59	Mean	298	640	0.9444	0.8738
		SD	32	58	0.0061	0.0114
3	97	Mean	319	317	0.9400	0.9328
		SD	35	30	0.0066	0.0063

4. Results and discussion

4.1. Training results

The results of training the DNN model using the three samples on both the training and validation sets is shown in Fig. 4 and summarized in Table 3. The MSE and R^2 accuracy scores are shown for all 10 runs to observe the scatter in these scores. In this figure, the scores are presented in blue and red for the training and validation sets respectively with a boxplot showing the median and the mean values, the interquartile range (IQR) between quartile 1 (25 %) and quartile 3 (75 %) and the data points lying outside of 1.5 times IQR (outliers).

Fig. 4 showed that increasing the number of points per curve from 8 in sample 1 to 15 in sample 2 increased the prediction accuracy of the training set. MSE reduced from 462 to 298 MPa^2, and R^2 increased from 0.9084 to 0.9444. The prediction accuracy for the validation set was also increased where MSE reduced from 820 to 640 MPa^2, and R^2 increased from 0.8249 to 0.8738.

Further increase in the number of points per curve to 26 in sample 3 slightly reduced the prediction accuracy of the training set while significantly increasing the prediction accuracy of the validation set. MSE values were 319 and 317 MPa^2, and R^2 score values were 0.9400

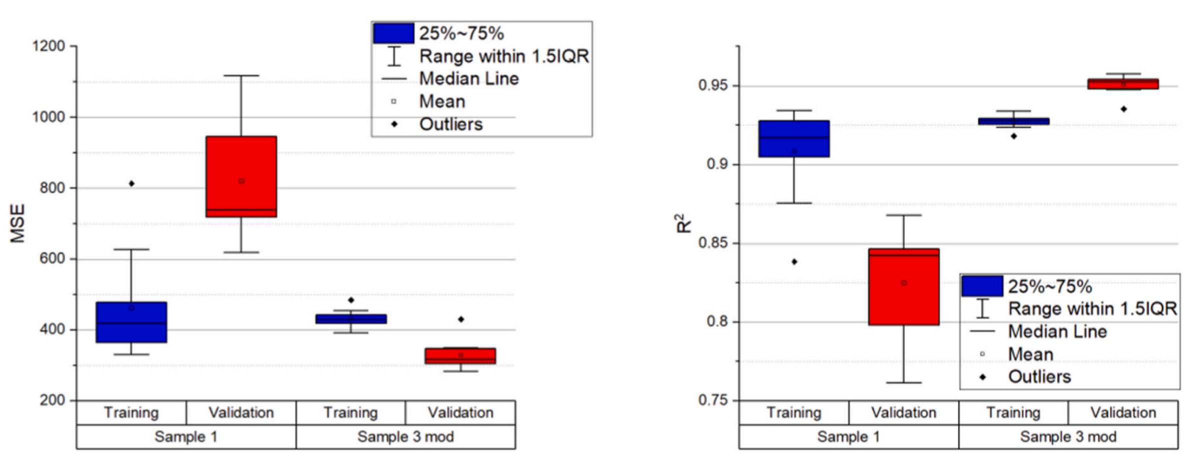

(a) (b)

Fig. 5. Accuracy scores for the prediction of the DNN on the training and validation sets using sample 3 mod compared to sample 1: (a) MSE, and (b) R^2.

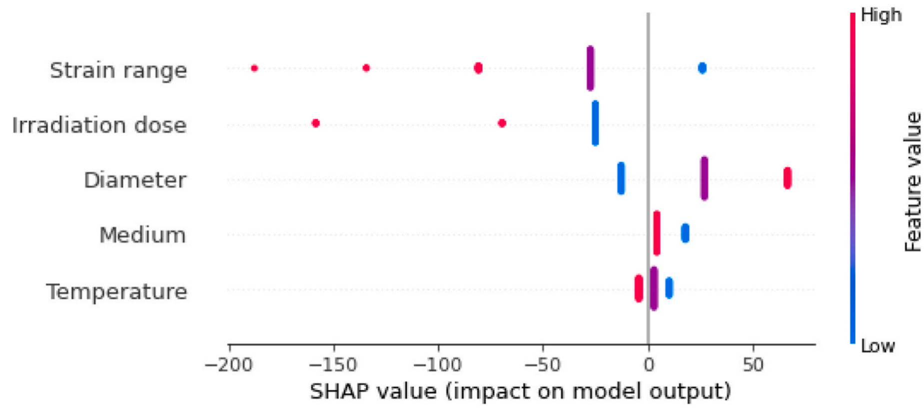

Fig. 6. SHAP analysis for the input variables using the DNN model trained using sample 3 as a reference model.

and 0.9328 for the training and validation sets respectively.

Another observation is that increasing the number of points per curve reduced the difference in the accuracy scores between the training and validation sets. We attribute this improvement to the reduction of overfitting of the training set. This proves that increasing the number of points per curve (from 8 to 26 in our case) improves the prediction of the cyclic softening behaviour of RAFM steels under unseen test conditions. Thus, sample 3 (26 points per curve) was chosen for the remaining investigation as the one achieving nearly the same accuracy for both sets.

The required computational time for the three samples is shown in Table 3. Obviously, enhancing the prediction accuracy of the DNN with increasing the number of points per curve increases the computational time. The running time increased by a factor 2.7 between samples 1 and 3. Yet still, the high running time of 97 s for sample 3 is very low compared to the alternative methods to predict the fatigue life discussed in the introduction. Avoiding the overfitting of the training set and the ability to predict the fatigue life on unseen test conditions is worth the longer running time.

The fact that increasing the number of points per curve enhanced the prediction accuracy of the validation set could be attributed to two reasons: increasing the whole sample size from 1280 to 4160 so with a larger training set size the accuracy was enhanced, or increasing the number of points per curve better defined the trend of these cyclic softening curves so the DNN model was able to learn this trend better. In order to address this point, a new sample was constructed with 26 points per curve similar to sample 3 and only 50 LCF tests. The new sample was thus called "sample 3 mod" with a total number of points of 1300 which is similar to sample 1. LCF tests were removed from each reference in order to keep a similar distribution of all the test conditions in this new database compared to the full database. The aim of this experiment is to verify which hypothesis applies in this case.

Sample 3 mod was split into training, validation, and prediction sets with the same ratio (70, 15, and 15 %) respectively. The DNN model with the same hyperparameters was then trained using the training set and the training, and validation sets accuracy scores were plotted for sample 3 mod and compared to sample 1. Fig. 5 shows the MSE and R^2 scores using sample 3 mod and sample 1.

Results show that using 26 points per curve with reduced LCF tests still enhanced the accuracy scores compared to 8 points per curve with the all the LCF tests. This further proves the point that proves the conclusion that increasing the number of points per curve helped the DNN model learn the trend of the cyclic softening curves and hence give better predictions.

4.2. Shapley Additive exPlanation (SHAP analysis)

SHAP analysis, based on the Shapley value proposed from game theory (Štrumbelj and Kononenko, 2013), was applied on the DNN model trained using sample 3 as a reference model. SHAP analysis is used to estimate the effect of each input variable on the target output. All the input variables except for p were included in this analysis with Q as the target variable. The decision to remove the accumulated plastic strain (p) from the analysis was due to the fact that its effect was quite significant making the effect of the rest of the parameters unclear. The effect of p could be observed on the cyclic softening curves of these RAFM steels with more pronounced cyclic softening as the accumulated inelastic strain increases. This was important to get insights on how the model analyses the effect of the different input variables on the cyclic softening behaviour which leads to better understanding of the model.

The results are displayed as a set of points representing each input feature in a separate row. The x-axis is the SHAP value which is the change of the predicted target from the mean of predictions. Negative values mean that the input feature lowers the predicted target and vice versa. The wider the spread of the points for a given variable, the more influence it has on the prediction. The colour of the point represents the value of the input variable ranging from red points for the highest values to blue points for the smallest values. The SHAP analysis results are shown in Fig. 6.

For example, consider the effect of strain range (the upper row in Fig. 6) on the target (cyclic softening) . For RAFM steels with non-Masing behaviour (Zahran et al., 2024), it is well-known that the higher the strain range, the more pronounced cyclic softening is (Oh et al., 2021b; Sarkar et al., 2014). In Fig. 6, higher strain ranges (shown with red points) correspond to more negative SHAP values, which means a negative effect on cyclic softening. Note that the notation in this manuscript is such that the lower the value of Q (negative), the more pronounced the cyclic softening is. Conversely, lower strain ranges (blue points) correspond to less negative or more positive SHAP values, indicating a positive effect on the target. Increasing the value Q means that the cyclic softening becomes less pronounced. SHAP analysis also shows that the second most significant factor is the irradiation dose: irradiated specimens show more pronounced cyclic softening compared to the non-irradiated specimens. This is similar to the observation by Materna-Morris et al. (2013).

The specimens with larger diameter showed less pronounced cyclic softening, with the effect of diameter being less significant than the two described above. One factor contributing to this effect is the fact that all LCF tests performed on irradiated specimens were done on specimens with smaller diameters (2 mm) compared to the non-irradiated specimens.

The least two significant inputs for the cyclic softening of RAFM steels were the test medium and the test temperature. According to the SHAP analysis, tests performed in air (represented by red SHAP points) showed slightly more pronounced cyclic softening compared to tests performed in vacuum (represented by blue SHAP points), while the

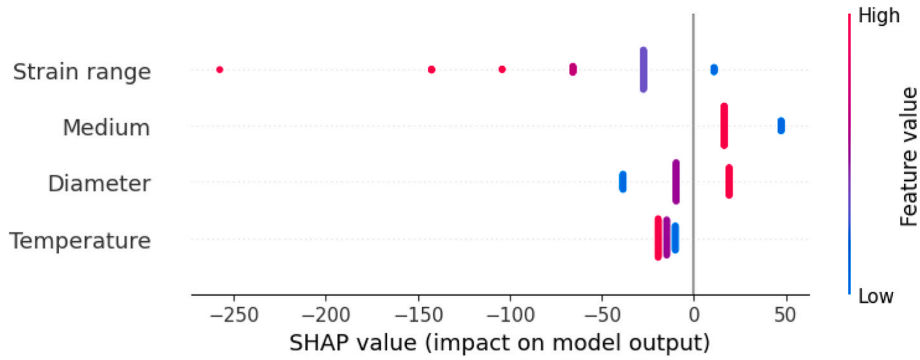

Fig. 7. SHAP analysis for the input variables using the DNN model trained using non-irradiated LCF specimens only in sample 3 as a reference model.

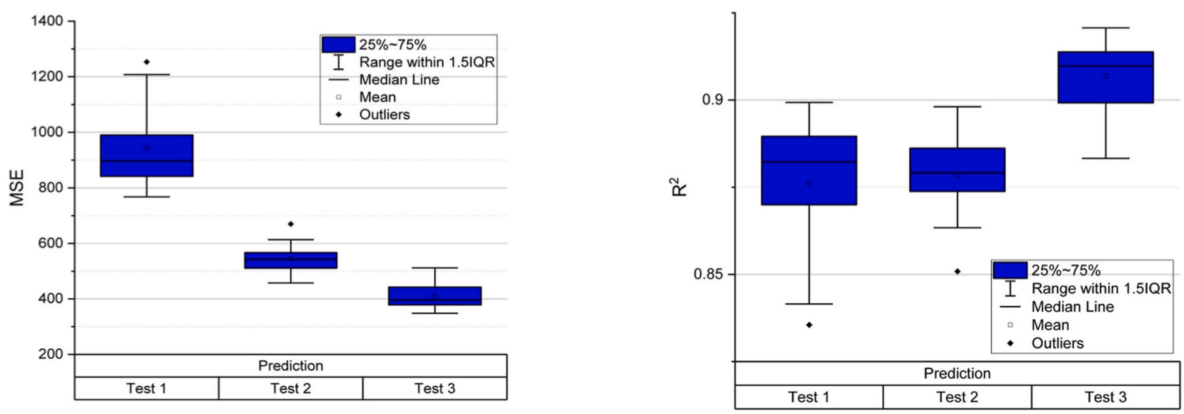

(a) (b)

Fig. 8. Accuracy scores for the prediction of the DNN on the prediction set: (a) MSE, and (b) R.^{2}.

higher the test temperature, the more pronounced cyclic softening.

The effect of specimen diameter on the cyclic softening behaviour of RAFM steels was further analysed to avoid the influence of the irradiated specimens of smaller diameters showing more pronounced cyclic softening. A separate SHAP analysis was applied on the model trained using the non-irradiated LCF specimens only in sample 3 (see Fig. 7). The SHAP analysis is shown in. Similar effects for all the different input variables was observed. This further strengthens the observations regarding how the DNN model analyses the effect of specimen diameter.

4.3. *Prediction of cyclic softening curves*

The ability of the DNN model to predict the cyclic softening curves under unseen test conditions was demonstrated through the prediction set. This set was not involved during the hyperparameter tuning or the training of the model. The accuracy of the model with the prediction set for the three samples is shown in Fig. 8. The MSE score was reduced from 944 MPa^2 – 408 MPa^2 between samples one and three. The R^2 score was also enhanced from 0.8761 to 0.9069 between both samples. This figure confirms that increasing the number of points per curve enhances the accuracy of the model, what we attribute to the reduction of the training data overfitting. The conclusion is that the model is capable not only of reproducing the values of cyclic softening from available LCF experiments but is also able to predict the cyclic softening curves of RAFM steels irradiated to doses for which no LCF tests have been carried out.

Sample 3 showed the best accuracy scores for the validation and prediction sets. Therefore, it was used to predict the cyclic softening curves of different RAFM steels and compared with the experimental curves from literature. The aim was to further show the accuracy of the prediction of the DNN model. Several test conditions were chosen from the validation set (not included in training the model) and the predicted vs experimental curves are shown in Figs. 9 and 10 for irradiated and non-irradiated specimens respectively. The figures showed very good comparison between the predicted and the experimental curves.

The cyclic softening behaviour of RAFM steels varies with the test conditions. As shown in section 4.2 that they experience more pronounced cyclic softening (more negative value of Q) for larger strain ranges. Fig. 9 shows that RAFM steels endure more accumulated plastic strains at smaller strain ranges. The advantage of using the DNN model is its ability to cover different ranges of accumulated plastic strains ranging from 7.5 to 50 in this figure.

After irradiation, RAFM steel experience pronounced cyclic softening at very small accumulated plastic strains. In Fig. 10a, the value of Q reaches −370 MPa at around 2.6 accumulated plastic strain. Again, the model was able to capture this change in cyclic softening behaviour after irradiation. This proves the capability of the model to predict the cyclic softening behaviour of irradiated and non-irradiated RAFM steels under different test conditions with high accuracy.

5. Conclusions

The aim of this work was to use ML to predict the cyclic softening curves of RAFM steels tested under different test conditions. This gives an alternative to performing LCF tests after neutron irradiation.

A DNN model with three hidden layers and 64 neurons per hidden layer was implemented and trained using the LCF test results gathered from literature. The model was used to predict the cyclic softening curves of irradiated and non-irradiated RAFM steels with high accuracy.

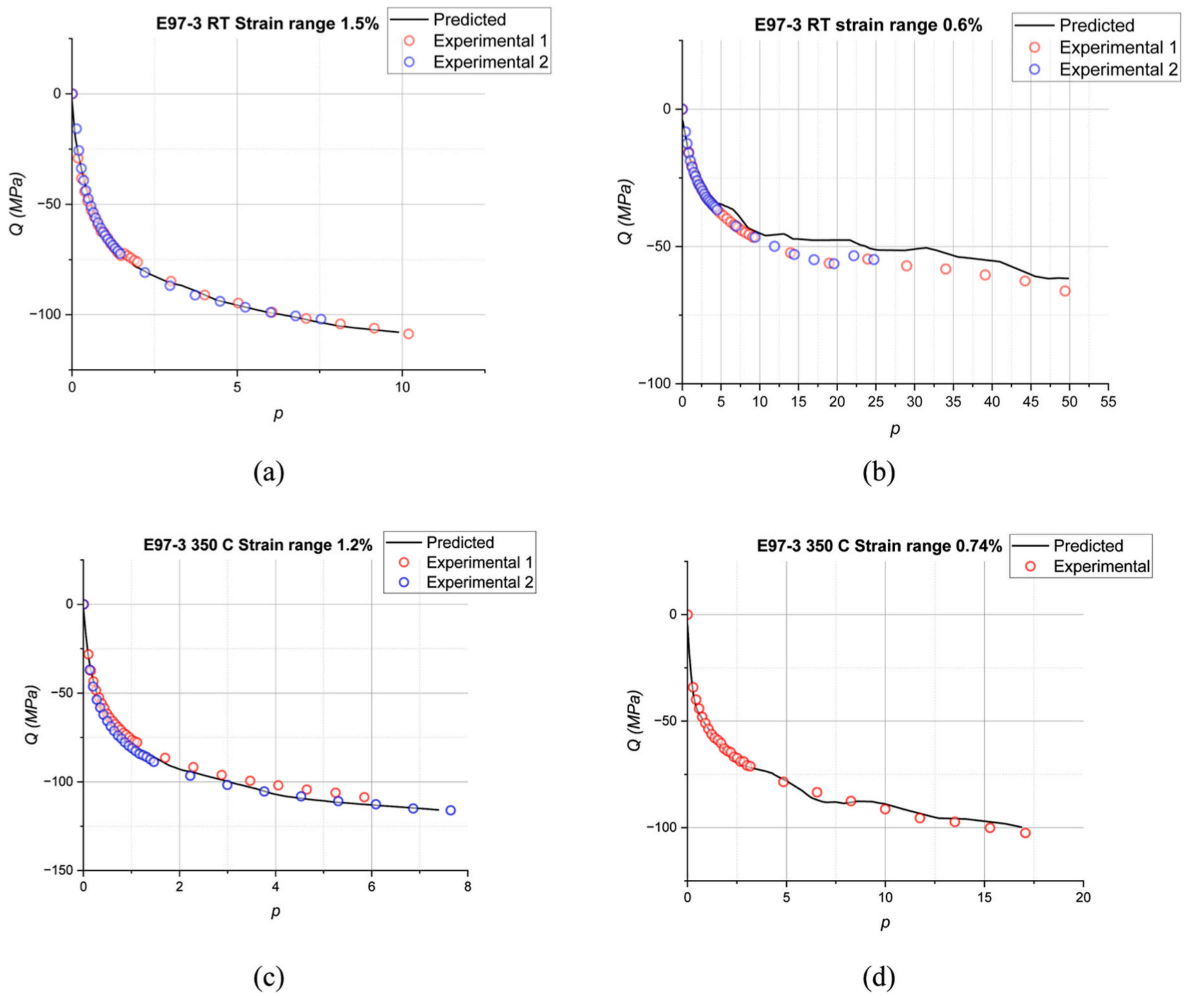

Fig. 9. Predicted cyclic softening curves of non-irradiated RAFM steels.

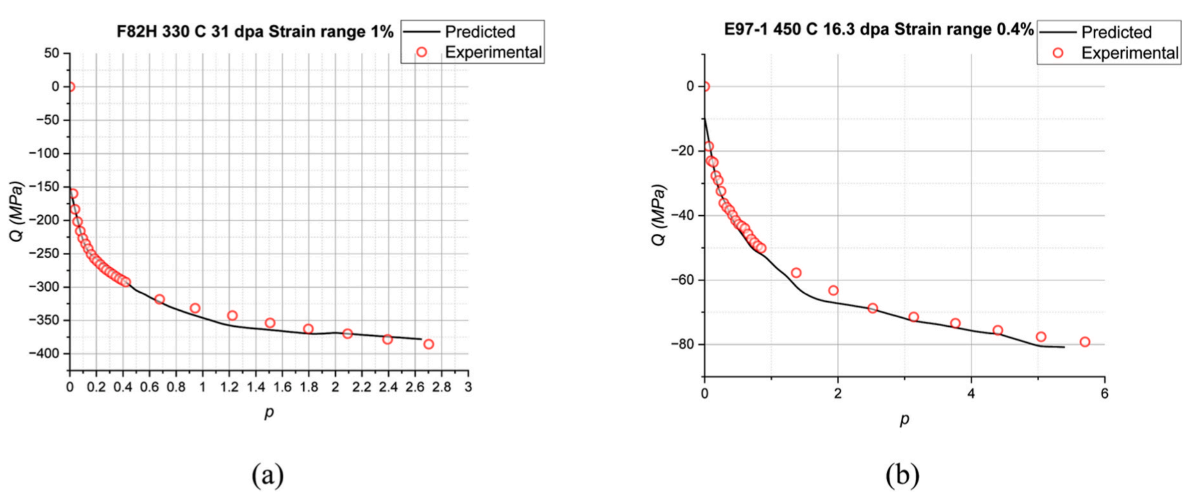

Fig. 10. Predicted cyclic softening curves of irradiated RAFM steels.

The main conclusions from this study are listed below.

- Using more points per cyclic softening curve in the training stage of the model implementation increased the validation accuracy. Training the model with sample 3 (26 points per curve) compared to sample 1 (8 points per curve) reduced the MSE score by a factor of 2.5 and increased the R^2 score by 13 %. This was attributed to the reduced overfitting of the training set. However, the increased accuracy came at the cost of increasing the running time by the factor of 2.7. Nevertheless, this number of points was considered optimal, because it resulted in nearly same accuracy score for the training and the validation sets.

- SHAP analysis showed that strain range, specimen diameter, and irradiation dose are the highest contributors to the cyclic softening of RAFM steels. On the other side, test temperature and test medium showed the lowest effect on cyclic softening.
- The DNN model was able to predict the cyclic softening curves at unseen test conditions with accuracy scores of 0.9069 and 408 MPa^2 for R^2 and MSE respectively.

CRediT authorship contribution statement

Hussein Zahran: Conceptualization, Methodology, Writing – original draft, Investigation, Software. **Aleksandr Zinovev:** Data curation, Writing – review & editing, Conceptualization, Supervision. **Dmitry Terentyev:** Funding acquisition, Writing – review & editing, Project administration. **Ali Aouf:** Software, Writing – review & editing. **Magd Abdel Wahab:** Writing – review & editing, Investigation, Supervision, Conceptualization.

Declaration of competing interest

The authors declare that they have no known competing financial interests or personal relationships that could have appeared to influence the work reported in this paper.

Acknowledgement

This work has been carried out within the framework of the EUROfusion Consortium, funded by the European Union via the Euratom Research and Training Programme (Grant Agreement No 101052200 — EUROfusion). Views and opinions expressed are however those of the author(s) only and do not necessarily reflect those of the European Union or the European Commission. Neither the European Union nor the European Commission can be held responsible for them. The work was also supported by FoD grant.

Data availability

Data will be made available on request.

References

Aktaa, J., Petersen, C., 2009a. Challenges in the constitutive modeling of the thermo-mechanical deformation and damage behavior of EUROFER 97. Eng. Fract. Mech. 76 (10), 1474–1484. https://doi.org/10.1016/j.engfracmech.2008.12.017.

Aktaa, J., Petersen, C., 2009b. Modeling the influence of high dose irradiation on the deformation and damage behavior of RAFM steels under low cycle fatigue conditions. J. Nucl. Mater. 389 (3), 432–435. https://doi.org/10.1016/j.jnucmat.2009.02.032.

Aktaa, J., Petersen, C., 2011. Modeling the constitutive behavior of RAFM steels under irradiation conditions. J. Nucl. Mater. 417 (1–3), 1123–1126. https://doi.org/10.1016/j.jnucmat.2010.12.295.

Aktaa, J., Schmitt, R., 2006. High temperature deformation and damage behavior of RAFM steels under low cycle fatigue loading: experiments and modeling. Fusion Eng. Des. 81 (19), 2221–2231. https://doi.org/10.1016/j.fusengdes.2006.03.002.

Aktaa, J., Walter, M., Angella, G., Cippo, E.P., 2019. Creep-fatigue design rules for cyclic softening steels. Int. J. Fatig. 118, 98–103. https://doi.org/10.1016/j.ijfatigue.2018.08.008.

Aktaa, J., Walter, M., Gaisina, E., Kolb, M.H.H., Knitter, R., 2020. Assessment of the chemical compatibility between EUROFER and ceramic breeder with respect to fatigue lifetime. Fusion Eng. Des. 157, 111732. https://doi.org/10.1016/j.fusengdes.2020.111732.

Albert, S.K., Laha, K., Bhaduri, A.K., Jayakumar, T., Rajendrakumar, E., 2016. Development of IN-RAFM steel and fabrication technologies for Indian TBM. Fusion Eng. Des. 109, 1422–1431. https://doi.org/10.1016/j.fusengdes.2015.12.005.

Barbosa, J.F., Correia, J.A.F.O., Freire, R.C.S., De Jesus, A.M.P., 2020a. Fatigue life prediction of metallic materials considering mean stress effects by means of an artificial neural network. Int. J. Fatig. 135. https://doi.org/10.1016/j.ijfatigue.2020.105527.

Barbosa, J.F., Correia, J.A.F.O., Júnior, R.C.S.F., Jesus, A.M.P.D., 2020b. Fatigue life prediction of metallic materials considering mean stress effects by means of an artificial neural network. Int. J. Fatig. 135. https://doi.org/10.1016/j.ijfatigue.2020.105527.

Bejani, M.M., Ghatee, M., 2021. A systematic review on overfitting control in shallow and deep neural networks. Artif. Intell. Rev. 54 (8), 6391–6438. https://doi.org/10.1007/s10462-021-09975-1.

Chernov, V.M., Leonteva-Smirnova, M.V., Potapenko, M.M., Budylkin, N.I., Devyatko, Y. N., Ioltoukhovskiy, A.G., Mironova, E.G., Shikov, A.K., Sivak, A.B., Yermolaev, G.N., Kalashnikov, A.N., Kuteev, B.V., Blokhin, A.I., Loginov, N.I., Romanov, V.A., Belyakov, V.A., Kirillov, I.R., Bulanova, T.M., Golovanov, V.N., Shamardin, V.K., Strebkov, Y.S., Tyumentsev, A.N., Kardashev, B.K., Mishin, O.V., Vasiliev, B.A., 2007. Structural materials for fusion power reactors -: the RF R&D activities. Nucl. Fusion 47 (8), 839–848. https://doi.org/10.1088/0029-5515/47/8/015.

de Albuquerque, V.H.C., Cortez, P.C., de Alexandria, A.R., Tavares, J.M.R.S., 2008. A new solution for automatic microstructures analysis from images based on a backpropagation artificial neural network. Nondestr. Test. Eval. 23 (4), 273–283. https://doi.org/10.1080/10589750802258986.

de Albuquerque, V.H.C., de Alexandria, A.R., Cortez, P.C., Tavares, J.M.R.S., 2009. Evaluation of multilayer perceptron and self-organizing map neural network topologies applied on microstructure segmentation from metallographic images. NDT E Int. 42 (7), 644–651. https://doi.org/10.1016/j.ndteint.2009.05.002.

Dong, Y., Yang, X., Chang, D., Li, Q., 2025. Predicting fatigue life of multi-defect materials using the fracture mechanics-based physics-informed neural network framework. Int. J. Fatig. 190. https://doi.org/10.1016/j.ijfatigue.2024.108626.

Farid, M., 2022. Data-driven method for real-time prediction and uncertainty quantification of fatigue failure under stochastic loading using artificial neural networks and Gaussian process regression. Int. J. Fatig. 155. https://doi.org/10.1016/j.ijfatigue.2021.106415.

Fernández, P., 2004. RAFM steel eurofer'97 as possible structural material for fusion device. Metallurgical characterization on as received condition and after simulated service conditions. Inorme técnico CIEMAT.

Führer, U., Aktaa, J., 2018. Modeling the cyclic softening and lifetime of ferritic-martensitic steels under creep-fatigue loading. Int. J. Mech. Sci. 136, 460–474. https://doi.org/10.1016/j.ijmecsci.2017.12.042.

Gaganidze, E., Petersen, C., 2011. Post Irradiation Examination of RAF/M Steels After Fast Reactor Irradiation up to 71 Dpa and < 340°C (ARBOR 2) : RAFM Steels: Metallurgical and Mechanical Characterisation., FZKA-7596, Institut Für Materialforschung II, Programm Kernfusion. Association Forschungszentrum Kalrsruhe/EURATOM, Germany. https://doi.org/10.5445/ksp/1000023594.

Gaganidze, E., Gillemot, F., Szenthe, I., Gorley, M., Rieth, M., Diegele, E., 2018. Development of EUROFER97 database and material property handbook. Fusion Eng. Des. 135, 9–14. https://doi.org/10.1016/j.fusengdes.2018.06.027.

Gao, J., Heng, F., Yuan, Y., Liu, Y., 2024. A novel machine learning method for multiaxial fatigue life prediction: improved adaptive neuro-fuzzy inference system. Int. J. Fatig. 178. https://doi.org/10.1016/j.ijfatigue.2023.108007.

Garcia, J.E.M., Pétesch, C., LebarbÉ, T., Bonne, D., Pascal, C., Blat, M., 2020. Design and construction rules for mechanical components of high-temperature, experimental and fusion nuclear installations: the RCC-MRx code last edition. Mechanical Engineering Journal 7 (4), 20. https://doi.org/10.1299/mej.20-00052, 00052–20–00052.

Giordana, M.F., Giroux, P.F., Alvarez-Armas, I., Sauzay, M., Armas, A., 2011a. Micromechanical modeling of the cyclic softening of EUROFER 97 steel. Procedia Eng. 10, 1268–1273. https://doi.org/10.1016/j.proeng.2011.04.211.

Giordana, M.F., Giroux, P.F., Alvarez-Armas, I., Sauzay, M., Armas, A., 2011b. Micromechanical modeling of the cyclic softening of EUROFER 97 steel. 11th International Conference on the Mechanical Behavior of Materials (Icm11) 10, 1268–1273. https://doi.org/10.1016/j.proeng.2011.04.211.

Halamka, J., Bartosák, M., Spaniel, M., 2023. Using hybrid physics-informed neural networks to predict lifetime under multiaxial fatigue loading. Eng. Fract. Mech. 289. https://doi.org/10.1016/j.engfracmech.2023.109351.

He, L., Wang, Z.L., Akebono, H., Sugeta, A., 2021. Machine learning-based predictions of fatigue life and fatigue limit for steels. J. Mater. Sci. Technol. 90, 9–19. https://doi.org/10.1016/j.jmst.2021.02.021.

Hirose, T., Sakasegawa, H., Nakajima, M., Kato, T., Miyazawa, T., Tanigawa, H., 2018. Effects of test environment on high temperature fatigue properties of reduced activation ferritic/martensitic steel. F82H, Fusion Engineering and Design 136, 1073–1076. https://doi.org/10.1016/j.fusengdes.2018.04.072.

Hu, X., Huang, L.X., Wang, W.G., Yang, Z.G., Sha, W., Wang, W., Yan, W., Shan, Y.Y., 2013. Low cycle fatigue properties of CLAM steel at room temperature. Fusion Eng. Des. 88 (11), 3050–3059. https://doi.org/10.1016/j.fusengdes.2013.08.001.

Hu, X., Huang, L.X., Yan, W., Wang, W., Sha, W., Shan, Y.Y., Yang, K., 2014. Low cycle fatigue properties of CLAM steel at 823 K. Mater. Sci. Eng. A Struct. Mater. Prop. Microstruct. Process. 613, 404–413. https://doi.org/10.1016/j.msea.2014.06.069.

Huang, Q.Y., Team, F., 2014. Development status of CLAM steel for fusion application. J. Nucl. Mater. 455 (1–3), 649–654. https://doi.org/10.1016/j.jnucmat.2014.08.055.

Jitsukawa, S., Tamura, M., van der Schaaf, B., Klueh, R.L., Alamo, A., Petersen, C., Schirra, M., Spaetig, P., Odette, G.R., Tavassoli, A.A., Shiba, K., Kohyama, A., Kimura, A., 2002. Development of an extensive database of mechanical and physical properties for reduced-activation martensitic steel F82H. J. Nucl. Mater. 307, 179–186. https://doi.org/10.1016/S0022-3115(02)01075-9.

Jung, Y., 2017. Multiple predicting K-fold cross-validation for model selection. J. Nonparametric Statistics 30 (1), 197–215. https://doi.org/10.1080/10485252.2017.1404598.

Kim, S.W., Tanigawa, H., Hirose, T., Kohayama, A., 2009. Cyclically induced softening in reduced activation ferritic/martensitic steel before and after neutron irradiation. J. Nucl. Mater. 386–88, 529–532. https://doi.org/10.1016/j.jnucmat.2008.12.168.

Lehnen, M., Aleynikova, K., Aleynikov, P.B., Campbell, D.J., Drewelow, P., Eidietis, N. W., Gasparyan, Y., Granetz, R.S., Gribov, Y., Hartmann, N., Hollmann, E.M., Izzo, V.

A., Jachmich, S., Kim, S.H., Kocan, M., Koslowski, H.R., Kovalenko, D., Kruezi, U., Loarte, A., Maruyama, S., Matthews, G.F., Parks, P.B., Pautasso, G., Pitts, R.A., Reux, C., Riccardo, V., Roccella, R., Snipes, J.A., Thornton, A.J., de Vries, P.C., Contributors, E.J., 2015. Disruptions in ITER and strategies for their control and mitigation. J. Nucl. Mater. 463, 39–48. https://doi.org/10.1016/j.jnucmat.2014.10.075.

Li, X.C., Zheng, M.J., Yang, X.Y., Chen, P.H., Ding, W.Y., 2022. A property-oriented design strategy of high-strength ductile RAFM steels based on machine learning. Mater. Sci. Eng. A Struct. Mater. Prop. Microstruct. Process. 840. https://doi.org/10.1016/j.msea.2022.142891.

Lian, Z.H., Li, M.J., Lu, W.C., 2022. Fatigue life prediction of aluminum alloy via knowledge-based machine learning. Int. J. Fatig. 157. https://doi.org/10.1016/j.ijfatigue.2021.106716.

Lindau, R., Möslang, A., Rieth, M., Klimiankou, M., Materna-Morris, E., Alamo, A., Tavassoli, A.A.F., Cayron, C., Lancha, A.M., Fernandez, P., Baluc, N., Schäublin, R., Diegele, E., Filacchioni, G., Rensman, J.W., van der Schaaf, B., Lucon, E., Dietz, W., 2005. Present development status of EUROFER and ODS-EUROFER for application in blanket concepts. Fusion Eng. Des. 75–79, 989–996. https://doi.org/10.1016/j.fusengdes.2005.06.186.

Liu, Y.C., Wu, H., Mayeshiba, T., Afflerbach, B., Jacobs, R., Perry, J., George, J., Cordell, J., Xia, J.Y., Yuan, H., Lorenson, A., Wu, H.T., Parker, M., Doshi, F., Politowicz, A., Xiao, L.D., Morgan, D., Wells, P., Almirall, N., Yamamoto, T., Odette, G.R., 2022. Machine learning predictions of irradiation embrittlement in reactor pressure vessel steels. npj Comput. Mater. 8 (1). https://doi.org/10.1038/s41524-022-00760-4.

Long, S.F., Zhao, M., 2020. Theoretical study of GDM-SA-SVR algorithm on RAFM steel. Artif. Intell. Rev. 53 (6), 4601–4623. https://doi.org/10.1007/s10462-020-09803-y.

Lopez, Z., Fatemi, A., 2012. A method of predicting cyclic stress-strain curve from tensile properties for steels. Mater. Sci. Eng. A Struct. Mater. Prop. Microstruct. Process. 556, 540–550. https://doi.org/10.1016/j.msea.2012.07.024.

Luzginova, N.V., Rensman, J., ten Pierick, P., Hegeman, J.B.J., 2011. Low cycle fatigue of irradiated and unirradiated Eurofer97 steel at 300°C. J. Nucl. Mater. 409 (2), 153–155. https://doi.org/10.1016/j.jnucmat.2010.09.017.

Mahler, M., Aktaa, J., 2018. Eurofer97 creep-fatigue assessment tool for ANSYS APDL and workbench. Nuclear Materials and Energy 15, 85–91. https://doi.org/10.1016/j.nme.2018.03.001.

Mariappan, K., Shankar, V., Sandhya, R., Laha, K., 2016. Low cycle fatigue design data for India-specific reduced activation ferritic-martensitic (IN-RAFM) steel. Fusion Eng. Des. 104, 76–83. https://doi.org/10.1016/j.fusengdes.2016.02.021.

Marmy, P., Kruml, T., 2008. Low cycle fatigue of eurofer 97. J. Nucl. Mater. 377 (1), 52–58. https://doi.org/10.1016/j.jnucmat.2008.02.054.

Materna-Morris, E., Möslang, A., Schneider, H.C., 2013. Tensile and low cycle fatigue properties of EUROFER97-steel after 16.3 dpa neutron irradiation at 523, 623 and 723 K. J. Nucl. Mater. 442 (1–3), S62–S66. https://doi.org/10.1016/j.jnucmat.2013.03.038.

Mergia, K., Boukos, N., 2008. Structural, thermal, electrical and magnetic properties of Eurofer 97 steel. J. Nucl. Mater. 373 (1–3), 1–8. https://doi.org/10.1016/j.jnucmat.2007.03.267.

Mortazavi, S.N.S., Ince, A., 2020. An artificial neural network modeling approach for short and long fatigue crack propagation. Comput. Mater. Sci. 185. https://doi.org/10.1016/j.commatsci.2020.109962.

Msolli, S., 2014. Thermoelastoviscoplastic modeling of RAFM steel JLF-1 using tensile and low cycle fatigue experiments. J. Nucl. Mater. 451 (1–3), 336–345. https://doi.org/10.1016/j.jnucmat.2014.04.020.

Muscat, M., Mollicone, P., You, J., Mantel, N., Jetter, M., 2023. Creep fatigue analysis of DEMO divertor components following the RCC-MRx design code. Fusion Eng. Des. 188. https://doi.org/10.1016/j.fusengdes.2023.113426.

Narendra, P.V.R., Prasad, K., Krishna, E.H., Kumar, V., Singh, K.D., 2019. Low-cycle-fatigue (LCF) behavior and cyclic plasticity modeling of E250A mild steel. Structures 20, 594–606. https://doi.org/10.1016/j.istruc.2019.06.014.

Nozawa, T., Tanigawa, H., Kojima, T., Itoh, T., Hiyoshi, N., Ohata, M., Kato, T., Ando, M., Nakajima, M., Hirose, T., Reed, J.D., Chen, X., Geringer, J.W., Katoh, Y., 2021. The status of the Japanese material properties handbook and the challenge to facilitate structural design criteria for DEMO in-vessel components. Nucl. Fusion 61 (11), 116054. https://doi.org/10.1088/1741-4326/ac269f.

Oh, Y.J., Ahiale, G.K., Chun, Y.B., Cho, S., Park, Y.H., Choi, W.D., Anderson, K.H.E., 2021a. Crystallographic evolution and cyclic softening behavior of reduced activation ferritic-martensitic steel under different fatigue modes. Mater. Sci. Eng. A Struct. Mater. Prop. Microstruct. Process. 802. https://doi.org/10.1016/j.msea.2020.140454.

Oh, Y.-J., Ahiale, G.K., Chun, Y.-B., Cho, S., Park, Y.-H., Choi, W.-D., Ebo Anderson, K.-H., 2021b. Crystallographic evolution and cyclic softening behavior of reduced activation ferritic-martensitic steel under different fatigue modes. Materials Science and Engineering: A 802. https://doi.org/10.1016/j.msea.2020.140454.

Paszke, A., Gross, S., Massa, F., Lerer, A., Bradbury, J., Chanan, G., Killeen, T., Lin, Z.M., Gimelshein, N., Antiga, L., Desmaison, A., Köpf, A., Yang, E., DeVito, Z., Raison, M., Tejani, A., Chilamkurthy, S., Steiner, B., Fang, L., Bai, J.J., Chintala, S., 2019. PyTorch: an imperative style, high-performance deep learning Library. Adv Neur In 32. https://doi.org/10.48550/arXiv.1912.01703.

Pedregosa, F., Varoquaux, G., Gramfort, A., Michel, V., Thirion, B., Grisel, O., Blondel, M., Prettenhofer, P., Weiss, R., Dubourg, V., Vanderplas, J., Passos, A., Cournapeau, D., Brucher, M., Perrot, M., Duchesnay, E., 2011. Scikit-learn: machine learning in python. J. Mach. Learn. Res. 12, 2825–2830.

Petersen, C., 2010. Post Irradiation Examination of RAF/M Steels After Fast Reactor Irradiation up to 33 Dpa and < 340^0C (ARBOR 1), FZKA-7517, Institut Für Materialforschung II, Programm Kernfusion ,Association Forschungszentrum Kalrsruhe. EURATOM, Germany. https://doi.org/10.5445/ir/270081166.

Pirjatullah, D. Kartini, Nugrahadi, D.T., Muliadi, Farmadi, A., 2021. Hyperparameter tuning using GridsearchCV on the comparison of the activation function of the ELM method to the classification of pneumonia in toddlers. 2021 4th International Conference on Computer and Informatics Engineering (Ic2Ie 2021), pp. 390–395. https://doi.org/10.1109/Ic2ie53219.2021.9649207.

Roldán, M., Leon-Gutierrez, E., Fernández, P., Gómez-Herrero, A., 2019. Deformation behaviour and microstructural evolution of EUROFER97-2 under low cycle fatigue conditions. Mater. Char. 158, 109943. https://doi.org/10.1016/j.matchar.2019.109943.

Sai, N.J., Rathore, P., Sridharan, K., Chauhan, A., 2023. Machine learning-based predictions of yield strength for neutron-irradiated ferritic/martensitic steels. Fusion Eng. Des. 195. https://doi.org/10.1016/j.fusengdes.2023.113964.

Sarkar, A., Vijayanand, V.D., Shankar, V., Parameswaran, P., Sandhya, R., Laha, K., Mathew, M.D., Jayakumar, T., Rajendrakumar, E., 2014. Cyclic softening as a parameter for prediction of remnant creep rupture life of a Indian reduced activation ferritic–martensitic (IN-RAFM) steel subjected to fatigue exposures. Fusion Eng. Des. 89 (12), 3159–3163. https://doi.org/10.1016/j.fusengdes.2014.10.004.

Spolladore, L., Rossi, R., Wyss, I., Gaudio, P., Murari, A., Gelfusa, M., Contributors, J., 2023. Detection of MARFEs using visible cameras for disruption prevention. Fusion Eng. Des. 190. https://doi.org/10.1016/j.fusengdes.2023.113507.

Štrumbelj, E., Kononenko, I., 2013. Explaining prediction models and individual predictions with feature contributions. Knowl. Inf. Syst. 41 (3), 647–665. https://doi.org/10.1007/s10115-013-0679-x.

Tanigawa, H., 2018. Technical challenges on material and design criteria development for fusion in-vessel components. Fusion Eng. Des. 133, 89–94. https://doi.org/10.1016/j.fusengdes.2018.05.047.

van der Schaaf, B., Tavassoli, F., Fazio, C., Rigal, E., Diegele, E., Lindau, R., LeMarois, G., 2003. The development of EUROFER reduced activation steel. Fusion Eng. Des. 69 (1–4), 197–203. https://doi.org/10.1016/s0920-3796(03)00337-5.

Wang, C., Shen, C., Cui, Q., Zhang, C., Xu, W., 2020a. Tensile property prediction by feature engineering guided machine learning in reduced activation ferritic/martensitic steels. J. Nucl. Mater. 529. https://doi.org/10.1016/j.jnucmat.2019.151823.

Wang, C.C., Shen, C.G., Huo, X.J., Zhang, C., Xu, W., 2020b. Design of comprehensive mechanical properties by machine learning and high-throughput optimization algorithm in RAFM steels. Nucl. Eng. Technol. 52 (5), 1008–1012. https://doi.org/10.1016/j.net.2019.10.014.

Wang, Y.J., Zhu, Z.Y., Sha, A.X., Hao, W.F., 2023. Low cycle fatigue life prediction of titanium alloy using genetic algorithm-optimized BP artificial neural network. Int. J. Fatig. 172. https://doi.org/10.1016/j.ijfatigue.2023.107609.

Wong, E.W.C., Kim, D.K., 2018. A simplified method to predict fatigue damage of TTR subjected to short-term VIV using artificial neural network. Adv. Eng. Software 126, 100–109. https://doi.org/10.1016/j.advengsoft.2018.09.011.

Zahran, H., Zinovev, A., Terentyev, D., Wang, X.W., Wahab, M.A., 2024. Experimental investigation and constitutive material modelling of low cycle fatigue of EUROFER97 for fusion applications. J. Nucl. Mater. 588. https://doi.org/10.1016/j.jnucmat.2023.154809.

Zhang, Z.P., Li, J., Sun, Q., Qiao, Y.J., Li, C.W., 2009. Two parameters describing cyclic hardening/softening behaviors of metallic materials. J. Mater. Eng. Perform. 18 (3), 237–244. https://doi.org/10.1007/s11665-008-9287-4.

Zhang, K., Walter, M., Aktaa, J., 2020. Ratcheting and fatigue behavior of Eurofer97 at high temperature, part 1: experiment. Fusion Eng. Des. 150, 111407. https://doi.org/10.1016/j.fusengdes.2019.111407.

Zhang, X.-C., Gong, J.-G., Xuan, F.-Z., 2021. A deep learning based life prediction method for components under creep, fatigue and creep-fatigue conditions. Int. J. Fatig. 148. https://doi.org/10.1016/j.ijfatigue.2021.106236.

Zhao, Y.Y., Zhai, X.W., Liu, S.J., 2016. Low cycle fatigue properties of CLAM steel at 450 °C and 550 °C. Fusion Eng. Des. 112, 213–217. https://doi.org/10.1016/j.fusengdes.2016.08.015.

Zhao, B., Song, J., Xie, L., Ma, H., Li, H., Ren, J., Sun, W., 2023. Multiaxial fatigue life prediction method based on the back-propagation neural network. Int. J. Fatig. 166. https://doi.org/10.1016/j.ijfatigue.2022.107274.

Zhou, J., Sun, Z., Kanouté, P., Retraint, D., 2018. Experimental analysis and constitutive modelling of cyclic behaviour of 316L steels including hardening/softening and strain range memory effect in LCF regime. Int. J. Plast. 107, 54–78. https://doi.org/10.1016/j.ijplas.2018.03.013.

Zhou, T., Jiang, S., Han, T., Zhu, S.-P., Cai, Y., 2023. A physically consistent framework for fatigue life prediction using probabilistic physics-informed neural network. Int. J. Fatig. 166. https://doi.org/10.1016/j.ijfatigue.2022.107234.

Zinovev, A., Lamagnere, P., Poleshchuk, K., Terentyev, D., Bernardi, D., Cristalli, C., Leon-Gutierrez, E., García-Rodríguez, N., Caes, C., Pintsuk, G., Aiello, G., 2024. Low cycle fatigue of EUROFER97 investigated for test blanket modules of ITER: an interlaboratory study. J. Nucl. Mater. 597. https://doi.org/10.1016/j.jnucmat.2024.155127.